The Flow Structure Inside a Microfabricated Inkjet Printhead

Carl D. Meinhart and Hongsheng Zhang

***Abstract*—A micrometer resolution particle image velocimetry system has been adapted to measure instantaneous velocity fields in an inkjet printhead. The technique uses 700-nm-diameter fluorescent flow tracing particles, a pulsed Nd : YAG laser, an epi-fluorescent microscope, and a cooled interline transfer charge-coupled device camera to record images of flow tracing particles at two known instances in time. Instantaneous velocity vector fields are obtained with spatial resolutions of 5–10 μm and temporal resolutions of 2–5 μs. The relationship between instantaneous velocity fields is compared to instantaneous shapes of the meniscus. The flow in the nozzle is highly unsteady and characterized by a maximum velocity of 8 ms^{-1}, Reynolds numbers of $\mathrm{Re} = 500$, and accelerations of up to 70 000 times gravity (i.e., 70 000 g). Since the flow field is periodic for each ejection cycle, the instantaneous measurements can be phased averaged to determine the evolution of the average flow field. The ejection cycle period is 500 μs, and consists of four primary phases: *infusion*, *inversion*, *ejection*, and *relaxation*. During infusion, the actuator plate is deflected downward creating a low pressure that draws fluid into the inkjet cavity through the orifice and pulls the meniscus into the cavity through the nozzle. The meniscus grows, begins to decrease in size, and then deforms in shape, becoming inverted for approximately 6 μs. The meniscus exits the cavity through the nozzle during droplet ejection. During relaxation, the flow undergoes viscously-damped oscillations, and reaches equilibrium before the next ejection cycle begins. [453]**

***Index Terms*—Inkjet, microfluidics, particle image velocimetry, PIV.**

I. Introduction

THE purpose of this paper is to extend the analysis of inkjet printheads by using an epi-fluorescent microscope to measure the evolution of the meniscus inside the inkjet, and use micrometer resolution particle image velocimetry (PIV) to measure detailed flow fields inside a SEAJet (static electricity actuator InkJET) nozzle, which is manufactured by the Seiko Epson Corporation, Matsumoto, Japan. The results of these measurements show the evolution of the flow field and its coupling to the meniscus during the ejection process.

Manuscript received June 4, 1999; revised October 29, 1999. An earlier version of this paper appeared in the ASME Symposium on MicroFluidics, International Mechanical Engineering Congress and Exposition. This work was supported by M. Hosokawa and M. Atobe, Seiko Epson Corporation, Matsumoto, Japan. This work was supported in part by the Defense Advanced Research Projects Agency under Grant F33615-98-1-2853. Subject Editor, W. N. Sharpe, Jr.

C. D. Meinhart is with the Department of Mechanical and Environmental Engineering, University of California at Santa Barbara, Santa Barbara, CA 93106 USA (e-mail: meinhart@engineering.ucsb.edu).

H. Zhang is with Trident Inc., Brookfield, CT 06804 USA (e-mail: hszhang@trident-itw.com).

Publisher Item Identifier S 1057-7157(00)02170-3.

A. Inkjet Background

Inkjet technology has become increasingly important during the past ten years, particularly because of its use in low-cost computer printers. The first commercial inkjet printers were introduced in the mid-1970's. These printers were expensive and plagued with reliability issues due to inkjet clogging. A major turning point in the industry occurred in 1984, when the Hewlett-Packard Company, Santa Rosa, CA, introduced the *Thinkjet* printer. The Thinkjet printer was the first product that used batch fabricated processes to produce low-cost disposable printheads, which allowed inkjet printers to be more practical because of reduced reliability issues [1]. Since the mid-1980's inkjet printers have been continually improved in quality and reliability, while being reduced in price. According to Kamisuki *et al.* [2], inkjet printers occupy 65% of the consumer printer market.

A recent market study published by the Network of Excellence in Multifunctional Microsystems (NEXUS) reported that the 1996 worldwide inkjet printer head market was 100 million units, with total sales of $4.4 billion. They projected that the 2002 worldwide inkjet printer head market would be 500 million units, with total sales of $10.0 billion [3].

The trend in inkjet printer technology is to increase printing quality and speed by: 1) reducing droplet size; 2) increasing the number of channels per head; 3) increasing ejection rates; and 4) reducing problems such as crosstalk between channels and satellite droplets [3], [4]. The quality of the ejection droplets is closely related to printing quality. In most situations, it is desirable to reduce droplet size, improve droplet consistency, and eliminate satellite droplets. Novel design concepts such as the virtual chamber neck can significantly improve droplet quality by eliminating satellite droplets [5].

In 1994, the state-of-the-art for inkjet technology was about 50–128 channels per head, with repetition rates of 3–6 kHz, and a resolution of 300–600 dpi [1]. This has been substantially improved in the past several years. The *Lexmark 7000* inkjet printer was introduced in 1998. It has 400 channels per head, with a repetition rate of 10 kHz, and a resolution of 1200 dpi [6].

A long-term design goal would be to develop inkjet printheads with 2500 nozzles per color at a resolution of 300 dpi. This would allow page-wide full-color printing, and would compete directly with high-end color laser printers. Unfortunately, this is beyond the limitations of current fabrication technology. Inkjets could be further improved by developing technology to modulate droplet size by, say, 8–16 levels [1].

B. Computational and Experimental Analysis of Inkjets

Most of the analysis of fluid flow inside inkjet nozzles has been limited to computational fluid dynamics (CFD) simulations. The CFD package *FLOW-3D* developed by Flow Sciences Inc., Los Alamos, NM, has been used for inkjet analysis by a significant number companies. Lexmark International Inc., Lexington, KY, used *FLOW-3D* to aid in the design of the 1200-dpi *Lexmark 7000*. The CFD simulations provided information that allowed engineers to determine what manufacturing tolerances were required to align printing dots to within 12.5 μm on a printed page [6].

Flow fields inside inkjet nozzles are difficult to simulate using CFD because of the complex boundary conditions associated with the problem. For instance, it is difficult to properly model the inkjet forcing mechanism. For thermal inkjets, the rate of heating and cooling of the fluid is related directly to the expansion and collapse of the evaporation bubble, which controls the displacement of the fluid within the cavity. In the Lexmark example, engineers modeled the actuation of the evaporation bubble using an internal code to predict the pressure field as a function of time, which was a forcing condition for the CFD simulation [6]. For nonthermal inkjets, such as the SEAJet, the motion of the actuator plate must be modeled accurately [2]. Since this motion is complicated and not well understood, it would be difficult to accurately simulate the flow in this type of device.

There have been a variety of experimental techniques used to examine the performance of inkjets. Poon and Lee [7] used a phase Doppler particle analyzer (PDPA) to determine the effect of crosstalk between adjacent nozzles, by measuring droplet size and velocity 4 mm away from the nozzle. They also used an optical vibrometer to measure the direction of motion of the meniscus inside the nozzle. The results showed that variations in drop volume were directly related to oscillations of the meniscus caused by crosstalk.

Tseng *et al.* [5] used an LED, a microscope, and a charge-coupled device (CCD) camera to record images of droplets with an approximate exposure time of 10 μs at a frequency of 1 kHz. The system allowed them to measure approximate droplet size, velocity, and number of droplets per ejection. They measured droplets ranging in size of 30–70 μm with velocities of 4.4–12 ms^{-1}. Their technique is useful for analyzing the droplet characteristics of many different types of inkjet nozzles.

Since bubble dynamics in thermal inkjets is closely associated with droplet volume and velocity, it is important to understand the evolution of the bubble during nucleation, growth, and collapse. Tsuchii *et al.* [8] measured the evolution of the bubble inside an inkjet cavity by measuring the acoustic emission (AE) wave generated by the vapor bubble. Their results showed that for the first 0.5 μs after the heater was activated, many small bubbles began to nucleate. Around 1 μs, the small bubbles began to combine into a single bubble. The single bubble continued to grow for about 8 μs before shrinking and finally collapsing around 20 μs. The bubble reappeared and then quickly collapsed again around 28 μs. The AE measurements showed that as the bubble collapsed, it had a higher pressure than when it nucleated. This high pressure could potentially damage the heating element in the inkjet.

C. Diagnostic Techniques for Microfluidics

During the past several years, a variety of techniques have emerged to measure flow fields in microfluidic devices. An overview of these techniques is given by Meinhart *et al.* [9]. These techniques include X-ray micro-imaging [10], optical Doppler tomography (ODT) [11], caged fluorescent streak velocimetry [12], particle streak velocimetry [13], and micrometer resolution PIV [14],[15].

Since the characteristic diameter of many inkjet nozzles are approximately 30–60 μm and the duration of droplet ejections are approximately 10–20 μs, fully resolved measurements of the flow field inside an inkjet nozzle require spatial resolutions of 5–10 μm and temporal resolutions of 2–5 μs. Most of the above diagnostic techniques have spatial resolutions ranging between 20–50 μm, with the exception of the micro PIV techniques, which have spatial resolutions ranging between 0.9–6.9 μm [9].

The only technique listed above that has a sufficient temporal resolution for measuring inkjet flows is the micro PIV technique described by Meinhart *et al.* [15]. This technique uses a set of two pulsed Nd : YAG lasers, to illuminate flow tracing fluorescent particles. The time-sequenced particle images are recorded by a $1030 \times 1300 \times 12$ bit cooled interline transfer CCD camera, which can record back-to-back images within 500 ns. The limitation of the CCD camera to record two consecutive images, combined with the duration of the laser pulses, determines the temporal resolution of the technique (i.e., the time required to obtain a velocity measurement). The temporal resolution of this micro-PIV technique is limited to 500 ns, which is sufficient for analysis of most inkjets.

II. Experimental Setup

A. SEAJet Nozzles

The printhead used in the current experiments is a SEAJet printhead [2]. The printhead is $10.97 \times 9.03 \times 2.10$ mm and is composed of three primary layers: a 100-μm-thick (100) silicon substrate and two 1-mm-thick Pyrex glass cover plates (see Fig. 1). The glass cover plates are anodically bonded to the top and bottom of the silicon wafer. Inkjet components such as nozzles, pressure plates, ink supply orifices, and ink cavities are micromachined directly into the silicon substrate using thermal oxidation and wet etching. Forming the bottom of the ink cavity is the pressure plate, which is a 13-μm-thick layer of silicon. The entrance of the cavity consists of an ink supply reservoir and orifices that restrict fluid motion through viscous resistance. A 6-μm-wide (on the top) and 45-μm-deep triangle-shaped nozzle is etched at the cavity exit. An electrode is formed under the pressure plate by depositing a 0.1-μm-thick ITO film. By applying a voltage across the electrode and pressure plate, an electrostatic force is generated, which deflects the pressure plate and induces fluid motion [2].

Fig. 1 illustrates the working mechanism of the SEAJet printhead. Fig. 1(a) shows the static condition of the printhead, when the pressure plate is undeflected and there is no ink motion within the nozzle or the cavity. A voltage is applied across the electrode and pressure plate, producing an electrostatic force that deflects the pressure plate [see Fig. 1(b)]. The deflecting

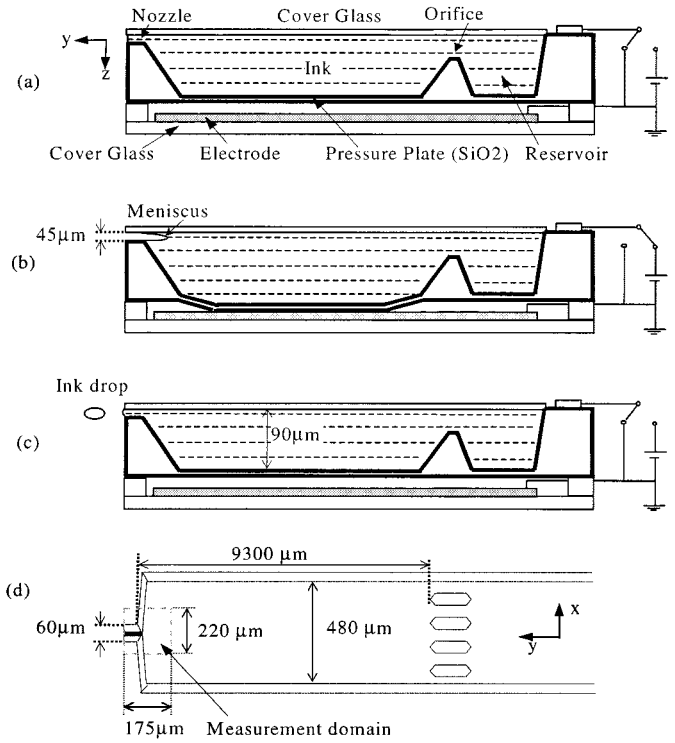

Fig. 1. Structure and working mechanism of the SEAJet printhead (adapted from Kamisuki *et al.* [2]). (a) Equilibrium position of pressure plate. (b) Deflected position of pressure plate when a 38-V potential is applied between the pressure plate and the electrode. (c) Equilibrium position of pressure plate as a drop is ejected through the nozzle, after the voltage across the plate is reduced to zero. (d) Top view of the SEAJet. The 200 μm $\times$ 175 μm box shows the size and position of the measurement domain.

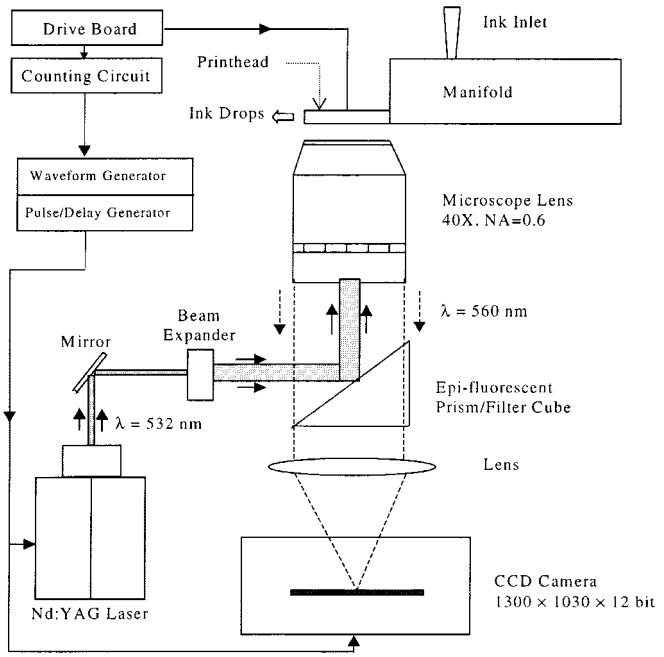

Fig. 2. Experimental apparatus. A drive board circuit is used to drive the SEAJet head. A counting circuit, pulse/delay generator and waveform generator are used to synchronize the PIV system and the drop ejection process. A doubled pulsed Nd : YAG laser is used to illuminate 0.7-μm-diameter flow tracing particles and the images are captured with a cooled interline transfer CCD camera.

plate pulls ink into the cavity from the reservoir through the orifice and pulls the meniscus into the cavity through the nozzle. When the voltage is reduced to zero, the pressure plate is released from the electrode and begins to vibrate about its equilibrium position inducing complex fluid motion. Fig. 1(c) shows the pressure plate at its equilibrium position while a droplet is being ejected from the nozzle.

For the current experiments, the SEAJet was electrically driven by a train of 2-kHz 38-V square wave pulses that was applied across the pressure plate and electrode. Each pulse had a duration of 32 μs and a period of 500 μs. The square wave pulses from the driving board were sent to the inkjet printhead and to a counting circuit, which triggered a waveform generator and a pulse generator that fired the Nd:YAG lasers and sequenced the CCD camera (see Fig. 2).

Even though flow transients due to inkjet startup occur during normal printing operations, the experiments reported in this paper were reference (i.e., time $t = 0$) from the beginning of the 25th square wave pulse. This provided a more consistent flow for analysis by eliminating flow transients resulting from inkjet startup, and produced flow conditions that were repeatable from cycle to cycle.

B. Flow Diagnostic System

Fig. 2 is a schematic of the PIV measurement system used in this study. The printhead is mounted on a movable x–y stage on an epi-fluorescent inverted microscope. A numerical aperture, $\mathrm{NA} = 0.6$, $40\times$ objective lens was positioned directly below the inkjet nozzle. A long working distance objective lens was required to image through the 1-mm-thick cover glass into the inkjet. The adjustable collar on the objective lens was required to compensate for optical aberrations between the glass/water interface. The object plane (i.e., the measurement plane) was precisely positioned relative to the inkjet by moving the objective lens vertically in the z-direction and by moving the stage horizontally in the x- and y-directions.

In PIV, velocity measurements are estimated by measuring the local displacement of particle images recorded at two known instances in time. As shown in Fig. 2, light from a set of pulsed Nd:YAG lasers is expanded and introduced into an epi-fluorescent attachment of an inverted microscope. The light is reflected by a prism and relayed through a $\mathrm{NA} = 0.6$, $40\times$ objective lens into the inkjet cavity. Fluorescently dyed 700-nm-diameter flow-tracing polystyrene particles absorb the green ($\lambda = 532$ nm) laser light and emit red ($\lambda \sim 560\,\mathrm{nm}$) light. The fluorescent light is imaged by the objective lens and passed through the epi-fluorescent filter cube, where green light from background reflections is removed. The red light is focused by a relay lens onto a cooled $1030 \times 1300 \times 12$ bit interline transfer CCD camera. A cooled CCD camera is required to record the low light levels emitted by the fluorescent particles. The interline transfer feature allows back-to-back recording of two images with a time delay of 500 ns [15]. The duration of a single laser light pulse combined with the decay time of the fluorescent dye was on the order of 5–10 ns, thereby freezing the motion of the particles. The time delay Δt between two successive exposures was chosen to be 2 and 5 μs, depending upon the characteristic velocity.

Deionized water seeded with 700-nm-diameter fluorescent polystyrene particles was introduced into the inkjet printhead reservoir through a Plexiglass manifold. The inkjet was filled by using high pressure to force fluid into the inkjet and remove the air bubbles. The printhead was mounted upside down, so that the inkjet cavity could be imaged through its upper glass plate by the inverted microscope (see Fig. 2).

The resulting fluorescent images were used to determine the structure of the flow field inside the inkjet by measuring instantaneous positions of the meniscus and instantaneous velocity fields. Since the measurements were repeatable from cycle to cycle, the instantaneous measurements could be phase averaged to determine the evolution of the flow structure throughout the ejection cycle.

The velocity measurements were obtained in a two–dimensional (2-D) plane centered 7 μm inside the cavity with a measurement depth of approximately 8–10 μm. The measurement depth was estimated as twice the distance from the object plane in which a particle becomes sufficiently unfocused so that it no longer contributes to the correlation function. The measurement depth depends on several factors, and is related to the depth of field of the objective lens [16].

C. Flow Tracing Particles

Since the velocity of the fluid is estimated by measuring the velocity of flow tracing particles, the accuracy of the measurements is ultimately limited by the fidelity in which the particles follow the flow. Assuming Stokes' drag, the difference between the particle and fluid velocities can be estimated by

$$|\mathbf{v}-\mathbf{u}| = \frac{\rho_p d_p^2 |\dot{v}|}{18\rho\nu} \tag{1}$$

where $\mathbf{v}$ is the particle velocity, $\mathbf{u}$ is the velocity of the fluid, $\dot{v}$ represents the total time derivative of the particle velocity, and ρ and ν are the density and kinematic viscosity of the fluid, respectively. The subscript p represents the properties of the particle [17]. The largest measured acceleration in the inkjet was $7.0\ \mathrm{E}+5\ \mathrm{ms}^{-2}$. Using polystyrene particles in water, which have a specific gravity of $\rho_p/\rho = 1.055$, and assuming a kinematic viscosity of $\nu = 1.006\ \mathrm{E}-6\ \mathrm{m}^2\mathrm{s}^{-1}$, a 700-nm-diameter particle will slip a maximum of $0.02\ \mathrm{m\ s}^{-1}$. With a full scale velocity of, say, $2\ \mathrm{ms}^{-1}$, the maximum full-scale error due to slip is approximately 1% FS. The slip velocity is, of course, much lower throughout most of the nozzle where the local flow field acceleration is much lower.

Following Santiago *et al.* [14], the error due to Brownian motion can be written as

$$\varepsilon_B = \frac{\langle s^2 \rangle^{1/2}}{\Delta x} = \frac{1}{u}\sqrt{\frac{2D}{\Delta t}} \tag{2}$$

where s^2 is the random mean square particle displacement associated with Brownian motion, D is the Brownian diffusion coefficient, and ν is the characteristic velocity. Using a characteristic velocity of $u = 1\ \mathrm{ms}^{-1}$ and a characteristic time delay of $\Delta t = 2\ \mu$s, the error due to Brownian motion of a 700-nm-diameter particle is less than 0.1%. This indicates that significantly smaller particles could be used without increasing error due to Brownian motion beyond acceptable levels.

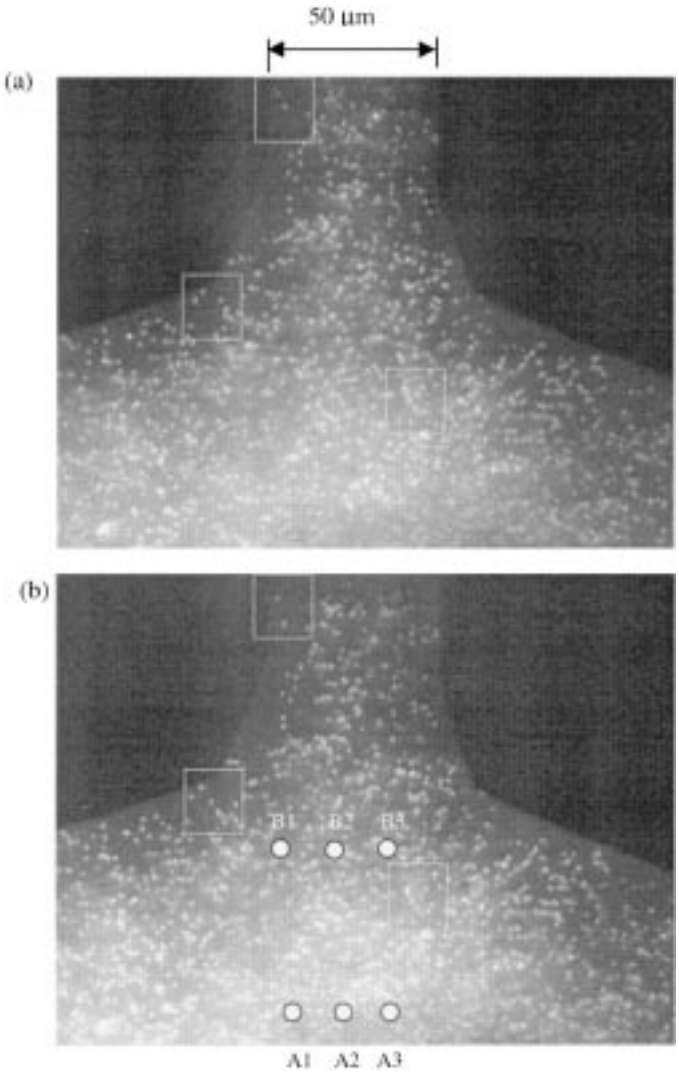

Fig. 3. An example of one pair of images ($\Delta t = 2\ \mu$s). Image (a) was taken at $t = 5\ \mu$s, and image (b) at $t = 7\ \mu$s. Particles within the three boxes demonstrate that the flow is toward the cavity. At each time, three velocities at positions A1, A2, and A3, and B1, B2, and B3 are measured and averaged. These average velocities are plotted against time for one ejection cycle in Fig. 4.

Seven hundred nanometer diameter particles were chosen because they were large enough to emit a sufficient amount of fluorescent light so that they could be imaged using the optical system shown in Fig. 2. Smaller particles would be more desirable, because the 700-nm-diameter particles were about 1/85th the size of the characteristic nozzle width ($\sim$60 μm). Further increases in particle size beyond 700-nm diameter would introduce errors resulting from particle/wall interactions. Generally, velocity measurements within approximately 2–5 particle diameters of the wall may be inaccurate because of particle/wall interactions.

III. Results

A typical pair of PIV images taken at times $t = 5\ \mu$s and $t = 7\ \mu$s is shown in Fig. 3. The particle concentration must be chosen judiciously so that there is a sufficient number of particle images for reliable signal in the PIV measurements without providing too much background noise. The three boxes in Fig. 3

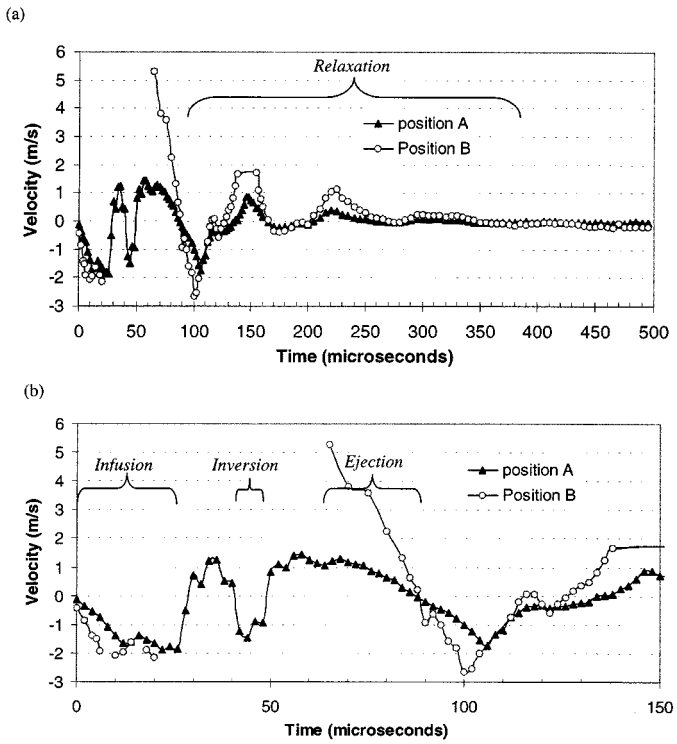

Fig. 4. The phased averaged axial (y-component) velocity profiles for spatial positions A and B. At each instance in time, the velocities at positions A and B are averaged over three measurement points A1, A2, and A3, and B1, B2, and B3, respectively (see Fig. 3). The velocity at each point is measured at a known time during many ejection cycles and phased-averaged to estimate the velocity profile. For reference, the electronic drive pulse is repeated every 500 μs, and has a duration of 32 μs. (a) Velocity profile showing the entire ejection cycle from time $t = 0$–500 μs. (b) Velocity profile showing details of the *infusion*, *inversion*, and *ejection* processes during times $t = 0$–150 μs.

depict recognizable groups of particles. From visual inspection of the boxes, one can deduce that there is motion of the fluid into the cavity during the 2-μs delay between Fig. 3(a) and (b). In order to characterize the bulk movement of the flow, two characteristic velocities are estimated by averaging the velocity at points A1, A2, and A3 (denoted as position A), and at points B1, B2, and B3 (denoted as position B). Position A was chosen as a characteristic position because that position is occupied by liquid throughout the entire ejection cycle, allowing velocity measurements to be obtained at all times during the cycle. Position B was chosen because it is closer to the nozzle entrance and provides velocity measurements throughout the cycle, except between times $20 < t < 65$ μs. In general, the profiles of A and B are roughly similar with B having a larger amplitude. Since the flow is periodic between ejection cycles, the instantaneous velocity fields can be phase averaged to form an estimate of the temporal evolution of the flow. The temporal evolution of velocities at positions A and B are shown in Fig. 4. Fig. 4(a) shows the entire 500-μs ejection cycle. Fig. 4(b) shows the velocity profiles during the actual ejection ($0 < t < 150$ μs).

During the first 27 μs of the cycle, the velocity starts at zero and becomes increasingly negative, reaching a minimum value of -2 ms^{-1}. This corresponds to the pressure plate deflecting downward drawing in fluid from the nozzle and reservoir. The fluid then accelerates from -2 ms^{-1} to approximately $+0.75$ ms^{-1} over a period of -4 μs. This corresponds to an

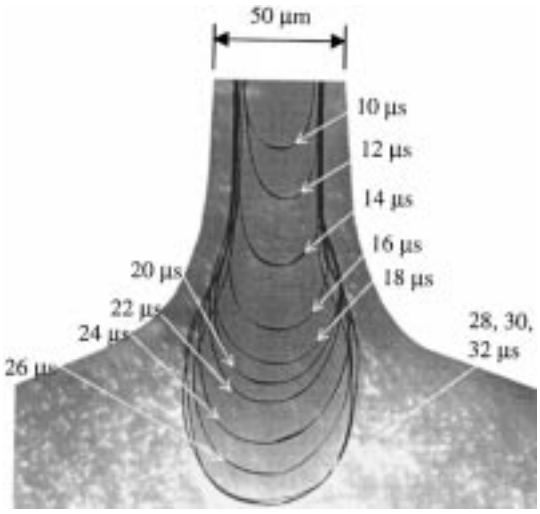

Fig. 5. Micrograph of meniscus shape from times $t = 10$–32 μs. Meniscus is growing toward the cavity as the pressure plate is deflected toward the electrode. The black lines represent the instantaneous position of the meniscus.

acceleration of -7 E $+ 5$ ms^{-2}, or 70 000 g. The velocity at A reaches a local maximum of 1.2 ms^{-1} at a time $t = 36$ μs, and decelerates reaching a local minimum of –1.5 ms^{-1} at $t = 46$ μs before reversing and reaching a maximum at $t = 58$ μs. At $t = 65$ μs, liquid occupies position B and velocity measurements can be obtained. The flow at B decelerates at -2.1 E $+ 5$ ms^{-2} from a maximum of 5.25 ms^{-1} at $t = 62$ μs to a minimum of –2.75 ms^{-1} at $t = 100$ μs. The magnitude of the flow field decays as it oscillates four more times with periods ranging between 75–100 μs. Images of the meniscus were taken at 2-μs intervals during the first 62 μs of the ejection cycle. The duration of each exposure was approximately 5–10 ns, which accounts for the 5-ns duration of the Nd : YAG laser pulse and the decay time of the fluorescence. Cycle-to-cycle repeatability of the experiment was tested by comparing images that were recorded at the same phase from two different cycles. The images appeared to be nearly identical, indicating that the experiment was highly repeatable between cycles.

At every 2 μs, the location of the meniscus was determined by carefully tracing the liquid/air interface. These traces were then superposed on each other to show the evolution of the meniscus. Fig. 5 shows the meniscus at times $t = 10$–32 μs. The meniscus grows as fluid is drawn into the cavity during times $t = 0$–28 μs, which corresponds to the negative velocity shown in Fig. 4. During this period, the meniscus is roughly elliptically shaped, with significant curvature at the center of the nozzle. From $t = 28$–32 μs, the meniscus remains roughly constant, corresponding to the large acceleration and near zero velocity exhibited in the velocity profile (see Figs. 4 and 5).

During time $t = 34$–62 μs, the meniscus displays complicated motion before it is pushed out of the inkjet cavity through the nozzle [see Fig. 6(a)–(d)]. From its maximum position, the meniscus retraces itself and decreases in size during $t = 34$–40 μs, corresponding to a local maximum in the velocity profile. Due to the complicated flow dynamics, spatial variations in the flow field, and a nonuniform pressure distribution, the center of the meniscus shape becomes inverted

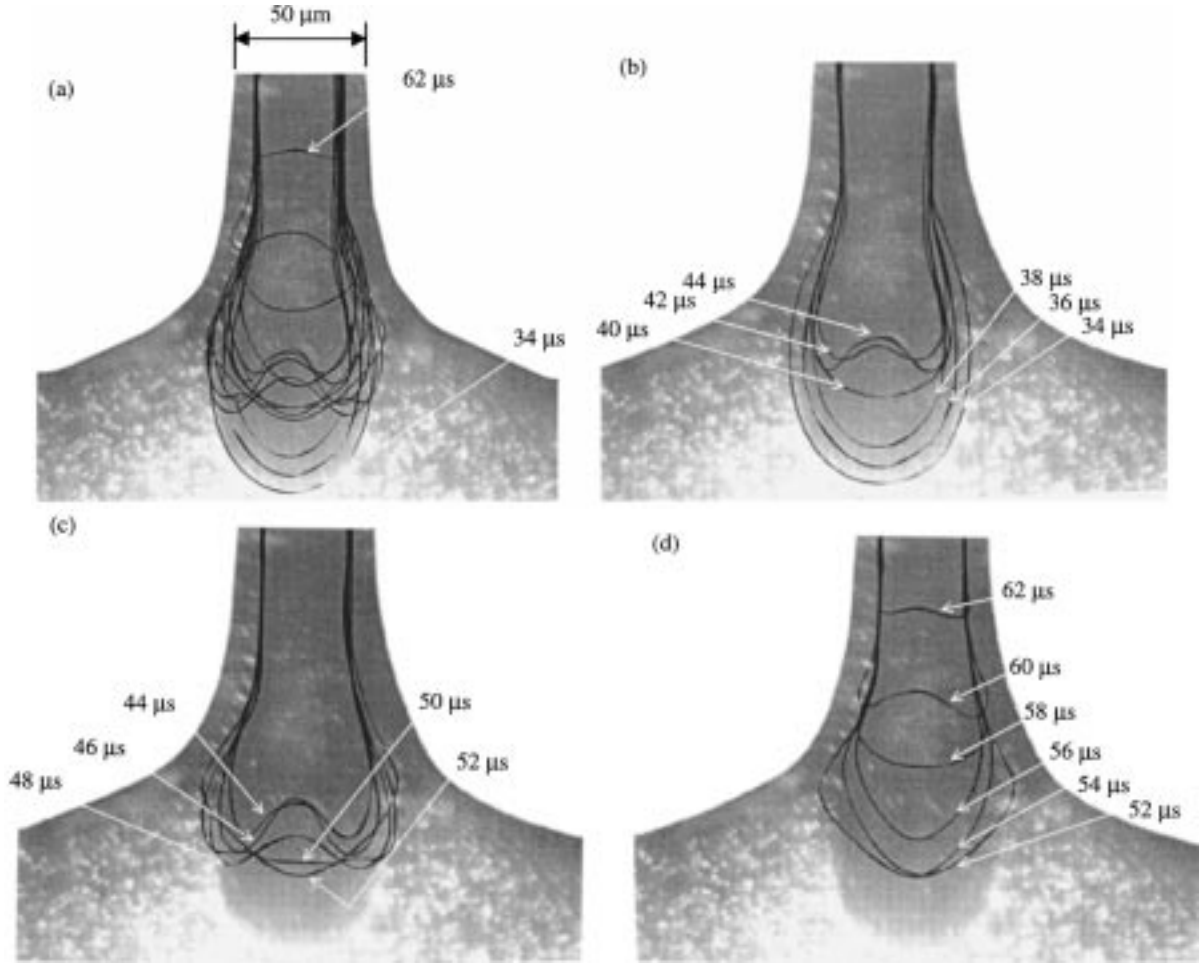

Fig. 6. Micrographs showing the complex motion of the meniscus as it decreases from a maximum size and is ejected through the nozzle. The meniscus positions are shown at 2-μs intervals. (a) Meniscus positions from times $t = 34$–62 μ s. (b) Meniscus positions as it is decaying from times $t = 34$–44 μs. (c) Meniscus positions during times $t = 44$–52 μs. (d) Meniscus positions just before being ejected through the nozzle during times $t = 52$–62 μs.

during $t = 42$–48 μs, which can be observed as a dip in the velocity profile. The meniscus inversion disappears completely by $t = 50$ μs. The meniscus becomes pointed at 54 μs, and is then flattened and pushed out of the cavity during times 58–62 μs, corresponding to the maximum in the velocity profile. The droplet ejection occurs when after meniscus exits the nozzle at $t = 62$ μs and before the velocity becomes negative at $t = 88$ μs.

Instantaneous velocity vector fields resulting from the PIV measurements are shown in Fig. 7(a)–(d) for times $t = 75$, 80, 85, and 90 μs. The spatial resolution of the measurements, based upon the size of the first interrogation window when projected back into the flow, was 8.16 μm $\times$ 22 μm, in the x- and y-directions, respectively. By overlapping the interrogation windows by 50%, the velocity vector spacing was 4 μm $\times$ 11 μm, in the x- and y-directions, respectively.

The vector field in Fig. 7(a), at time $t = 75$ μs, shows the flow moving out of the nozzle during droplet ejection. The flow velocity is a maximum near the center of the nozzle and decreases close to zero away from the center line. The velocity of the fluid in the nozzle reaches a maximum velocity of 8 ms^{-1}, corresponding to a Reynolds number based on nozzle width of $\mathrm{Re} = 500$. At time $t = 80$ μs, the flow field is still directed out of the cavity, but is lower in magnitude [see Fig. 7(b)]. The flow field reversal can be observed in Fig. 7(c) at $t = 85$ μs. At this instant in time, flow in the middle of the nozzle is moving out of the cavity, while the flow near the edges of the nozzle is moving into the cavity. This variation in the flow through the nozzle may contribute to the formation of nonuniform droplets. By time $t = 90$ μs, the flow has completely reversed [Fig. 7(d)].

IV. Discussion

Since the measurement plane is centered inside the inkjet cavity at approximately 7 μm from the planar coverslip, the flow at the measurement plane is nearly 2-D and does not exhibit a significant amount of out-of-plane motion. At positions farther away from the wall, one would expect the flow field to have a similar behavior to the current measurements, but with significantly more out-of-plane motion and perhaps larger variations in velocity.

The velocity profiles shown in Fig. 4 are highly transient, with velocity values changing significantly over time periods as short as a few microseconds and with accelerations on the order of 70 000 g. Due to this highly transient behavior, the small scale deviations in the velocity profiles, shown in Fig. 4(b), most likely result from random variations in the experiment.

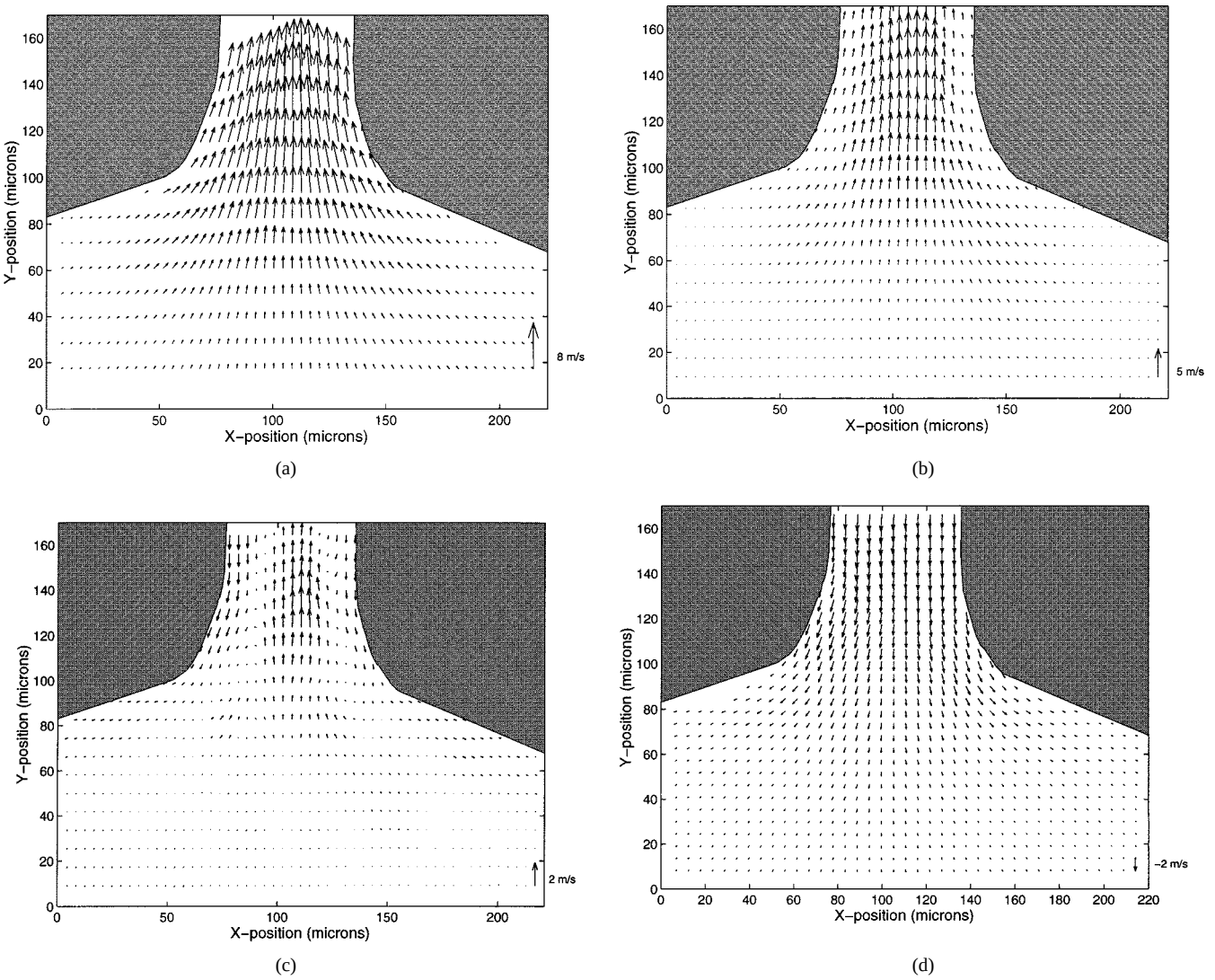

Fig. 7. Velocity vector fields showing the flow structure near the nozzle during and immediately following fluid ejection. The velocity fields are measured using micron resolution PIV. The spatial resolution (defined by the size of the first interrogation window) is 8.16 μm $\times$ 22 μm in the x- and y-directions, respectively. (a) Velocity field at time $t = 75$ μs shows fluid being ejected through the nozzle. (b) Velocity field at time $t = 80$ μs shows the flow rate decreasing. (c) Velocity field at time $t = 85$ μs shows the initial stages of flow reversal. (d) Velocity field at time $t = 90$ μs shows complete flow reversal after fluid ejection.

Following the observations resulting from Figs. 4–7, four distinct regimes of the ejection cycle can be identified: *infusion*, *inversion*, *ejection*, and *relaxation*. The first regime, *infusion*, occurs from times $t = 0$–28 μs. During infusion, the pressure plate is deflected, pulling fluid into the cavity through the orifice and pulling the meniscus into the cavity. The meniscus size is a maximum at the end of the *infusion* regime. The meniscus decreases in size, and then becomes inverted during the *inversion* regime, at times $t = 42$–48 μs. During this regime, the pressure plate is released from the electrode and begins moving back towards equilibrium. The inflow from the orifice impacts on the center of the meniscus, creating the inversion. Surface tension at the interface tries to minimize the surface area of the meniscus, removing the inversion by $t = 50$ μs.

During the *ejection* regime, at times $t = 62$–88 μs, the velocity inside the nozzle reaches a maximum of 8 ms^{-1}. In terms of droplet quality, this is a critical regime. Ideally, the flow should have a sharp pulse of high velocity and then a quick reversal. If a clean break does not occur between the primary droplet and the fluid in the nozzle, satellite droplets occur. Fig. 7(c) shows that the flow near the edges of the nozzle is reversed, the flow near the center of the nozzle is still moving out of the cavity. This spatial variation of the flow in the nozzle contributes to the formation of nonuniform droplets.

The flow exhibits several decaying oscillations during the *relaxation* regime. These oscillations are caused by the residual motion of the pressure plate, coupled with the inertia of the fluid in the cavity, and the resistance of the flow through the orifice and the meniscus. In principle, the duration of the oscillations can be reduced by increasing the viscosity of the fluid in the cavity.

The trend for inkjet technology is to increase the repetition rate of the inkjet. The current experiments were run at a repetition rate of 2 kHz (i.e., a period of 500 μs). From Fig. 4(a), the relaxation regime gradually decreases, but still has a finite value at time $t = 325$ μs. If the desired repetition rate is, say,

5 kHz, then the ejection and relaxation regimes must be significantly reduced. The relaxation regime should finish by time $t < 150$ μs, to avoid contamination of subsequent pulses. One way to decrease the time scale of the ejection cycle is to reduce the length scale of the inkjet. The period of the relaxation regime can be decreased by increasing the thickness and/or decreasing the lateral size of the pressure plate.

One potential method for improving ejection quality is to modify the nozzle shape. The current inkjet nozzle is fabricated by anisotropically etched (100) silicon [2]. Subsequently, there is little control on nozzle shape with this fabrication process. Fig. 7(c) shows that the flow does not reverse uniformly in the nozzle. Potentially, flow reversal could be more distinct by modifying the surface coating of the nozzle. This would alter the fluid boundary condition inside the nozzle, and may produce a more uniform flow reversal. The effectiveness of different surface coatings can be evaluated using the micro PIV technique.

V. Conclusions

Micrometer resolution PIV has been used for the first time to measure the instantaneous flow structure inside a commercially available inkjet printhead. The technique was used to measure instantaneous velocity vector fields at approximately 1000 points inside the inkjet cavity and the instantaneous shape of the meniscus. The spatial resolution of the PIV measurements, based upon the size of the first interrogation window when projected back into the flow, was 8.16 μm $\times$ 22 μm. By overlapping the interrogation windows by 50%, the velocity vector spacing was 4 μm $\times$ 11 μm. The thickness of the measurement plane was estimated to be about 8–10 μm and centered about 7 μm inside the inkjet cavity. The time delay between the two image exposures (i.e., temporal resolution) ranged between $\Delta t = 2$–5 μs, depending upon the characteristic flow velocity.

The flow field and meniscus shapes in the nozzle were shown to be periodic from cycle to cycle. The flow near the nozzle is characterized by large accelerations with a maximum of $7\,\mathrm{E}+5$ ms^{-2} (i.e., 70 000 g), which occurs immediately after the meniscus reaches a maximum size at the time $t = 28\,\mu$s. The velocity of the fluid in the nozzle reaches a maximum of 8 m s^{-1}. This corresponds to a Reynolds number based on nozzle width of $\mathrm{Re} = 500$.

Four distinct regions of the ejection cycle have been identified: *infusion*, *inversion*, *ejection*, and *relaxation*. During infusion, the inkjet pressure plate is deflected downward, drawing the meniscus into the cavity during the first 28 μs of the ejection cycle. The meniscus maintains a constant shape during times 28–32 μs. The meniscus then retraces itself and decreases in size during times 34–40 μs. Due to the complicated inkjet flow dynamics, spatial variations in the flow field, and a nonuniform pressure distribution, the center of the meniscus shape becomes inverted during times 42–48 μs. The meniscus inversion disappears completely by time 50 μs, and is pushed out of the cavity during times 58–62 μs, just before droplet ejection.

Acknowledgment

The authors would like to thank Dr. S. Wereley for his helpful suggestions throughout this research project.

References

[1] R. N. Mills, "Ink jet printing—Past, present and future," in *Proc. IS&T 10th Int. Cong. Advances Non-Impact Printing Technol.*, New Orleans, LA, Nov. 4, 1994.
[2] S. Kamisuki, T. Hagata, C. Tezuka, Y. Nose, M. Fujii, and M. Atobe, "A low power, small, electrostatically driven commercial inkjet head," in *Proc. IEEE MEMS Workshop*, Heidelberg, Germany, Jan. 25–29, 1998.
[3] S. Marshall, C. R. Hassett-Walker, I. Papautsky, and T. Roessing, "Nexus market analysis task force issues market study report on MEMS/MST," *Micromachine Devices Newslett.*, vol. 3, no. 10, Oct. 1998.
[4] C. C. Beatty, "A chronology of thermal ink-jet structures," in *Proc. Solid-State Sens. Actuators Workshop*, Hilton Head, SC, June 13–16, 1996.
[5] F.-G. Tseng, C.-J. Kim, and C.-M. Ho, "A novel microinjector with virtual chamber neck," in *Proc. IEEE MEMS Workshop*, Heidelberg, Germany, Jan. 25–29, 1998.
[6] D. Deitz, "Connecting the dots with CFD," *Mech. Eng. Mag.*, Mar. 1998.
[7] C. C. Poon and F. C. Lee, "Crosstalk study of a thermal inkjet print head from real-time drop size and velocity measurements," in *Proc. IS&T 9th Int. Cong. Advances in Non-Impact Printing Technol.*, Yokohama, Japan, Oct. 4–8, 1993.
[8] K. Tsuchii, Y. Tamura, A. Asai , and H. Yaegashi, "Analysis of bubble pressure bubble jet printing technology," in *Proc. IS&T 9th Int. Cong. Advances Non-Impact Printing Technol.*, Yokohama, Japan, Oct 4–8, 1993.
[9] C. D. Meinhart, S. T. Wereley, and J. G. Santiago, "Micron-resolution velocimetry techniques," in *Develop. Laser Tech. Applicat. Fluid Mechan.*, R. J. Adrian *et al.*, Eds. Berlin, Germany: Springer-Verlag, 1999.
[10] A. M. Lanzillotto, T. S. Leu, M. Amabile, R. Wildes, and J. Dunsmuir, "Applications of X-ray micro-imaging, visualization and motion analysis techniques to fluidic microsystems," in *Proc. Solid-State Sens. Actuators Workshop*, Hilton Head, SC, June 13–16, 1996.
[11] Z. Chen, T. E. Milner, D. Dave, and J. S. Nelson, "Optical Doppler tomographic imaging of fluid flow velocity in highly scattering media," *Opt. Lett.*, vol. 22, pp. 64–66, 1997.
[12] P. H. Paul, M. G. Garguilo, and D. J. Rakestraw, "Imaging of pressure- and electrokinetically-driven flows through open capillaries," *Anal. Chem.*, vol. 70, no. 13, 1998.
[13] J. P. Brody, P. Yager, R. E. Goldstein, and R. H. Austin, "Biotechnology at low Reynolds numbers," *Biophys. J.*, vol. 71, pp. 3430–3441, 1996.
[14] J. G. Santiago, S. Wereley, C. D. Meinhart, D. J. Beebe, and R. J. Adrian, "A micro particle image velocimetry system," *Exp. Fluids*, vol. 25, no. 4, pp. 316–319, 1998.
[15] C. D. Meinhart, S. T. Wereley, and J. G. Santiago, "PIV measurements of a microchannel flow," *Exp. Fluids*, vol. 27, no. 5, pp. 414–419, 1999.
[16] S. T. Wereley and C. D. Meinhart, "Volume illuminated particle image velocimetry," in *Proc. 3rd Int. Workshop Particle Image Velocimetry*, Santa Barbara, CA, Sept. 16–18, 1999, pp. 545–550.
[17] R. J. Adrian, "Particle-imaging techniques for experimental fluid mechanics," *Annu. Rev. Fluid Mech.*, vol. 23, pp. 261–304, 1991.

Carl D. Meinhart received the BS, MS, and Ph.D degrees from the University of Illinois at Urbana-Champaign, in 1989, 1991, and 1994, respectively. His Ph.D. research involved the investigation of coherent structures in wall-bounded turbulent flows.

Prior to joining the faculty of the University of California at Santa Barbara (UCSB) in 1996, he spent one year as a Post-Doctoral Researcher at the University of Illinois at Urbana-Champaign, and one year as a Research Engineer at the Ford Motor Company, Dearborn, MI. Since joining the faculty at UCSB, his research has focused on developing and applying diagnostic techniques to study transport phenomena in microfluidic devices.

Hongsheng Zhang received the BSME and MSME degrees from China, in 1994 and 1997, respectively, and the Master's degree in mechanical engineering from University of California at Santa Barbara, in 1999.

He is currently an Inkjet Development Engineer with Trident Inc., Brookfield, CT. He has co-authored four technical papers. He research experience is in inkjet technologies, fluid mechanics, thermal science, and PIV.